Available online at www.sciencedirect.com
SCIENCE DIRECT®
Journal of Magnetic Resonance 159 (2002) 62–67
JMR Journal of Magnetic Resonance
www.academicpress.com

Spin interaction filter in solid-state NMR Imaging

C. Casieri[a] and F. De Luca[b,*]

[a] INFM and Dipartimento di Fisica, Universita' dell'Aquila, I-67100 L'Aquila, Italy
[b] INFM and Dipartimento di Fisica, Universita' La Sapienza, I-00185 Rome, Italy

Received 7 May 2002; revised 29 July 2002

Abstract

In the tilted rotating frame (TRF), the transverse relaxation time $T_{2\rho}$ depends strongly on the orientation of TRF with respect to the usual rotating frame. In the spin space, the relative orientation of the two reference frames modifies the contribution of various spin interactions to $T_{2\rho}$ relaxation. Since the orientation of the frames and, to some extent, the role of the spin Hamiltonians in TRF are controllable experimentally, the $T_{2\rho}$ relaxation can be made sensitive to molecular mechanisms related to the selected spin interaction. In this paper, the realization of a contrast Hamiltonian-dependent in solid-state NMR Imaging is proved. The solid-state imaging approach is based on the magic angle in the rotating frame. Some results on simple solid polymers are presented.

1. Introduction

Among the NMR Imaging parameters used for solid-state imaging contrast [1,2], those relative to the relaxation in the rotating frame (RF) are particularly efficient [3,4], especially $T_{2\rho}$. Although it shares many aspects with $T_{1\rho}$, it presents some features very interesting both for imaging and relaxometry [5].

A peculiar aspect of the transverse tilted rotating frame (TRF) relaxation concerns the form that its zero frequency term assumes in the $T_{2\rho}$ frequency-dependent dispersion. The activity of the zero term is, in fact, dependent on the Wigner matrix elements that "project" the secular spin Hamiltonian in the TRF. These matrix elements depend, in turn, on the angles that set the orientation of TRF (TRF: $x'y'z'$, where $B_E\hat{z}'$ and B_E is the effective Zeeman magnetic field) with respect to RF (RF: xyz, where $B_0\hat{z}$ and B_0 is the main magnetic field). With the set of Euler angles $\alpha = \omega t$, $\theta = tg^{-1}[\gamma B_1/(\omega_0 - \omega)]$, and

$$\beta = \omega_E t = \gamma B_E t = \gamma \left[\left(\frac{\omega_0 - \omega}{\gamma} \right)^2 + B_1^2 \right]^{1/2} t,$$

where $\omega \cong \omega_0 = \gamma B_0$ is the frequency of the radio frequency field $2B_1 \cos \omega t$, the generic spin Hamiltonian in the TRF can be easily written as

$$H_{TRF} = \sum_{mm'} (-1)^m e^{-im'\alpha} d^{(l)}_{m'm}(\theta) e^{-im\beta} A_{lm} F_{l-m}(t), \tag{1}$$

where A_{lm} and F_{lm} are irreducible l-rank spherical tensors which depend on spin and random coordinates and

$$\begin{aligned} d^{(2)}_{00} &= -\tfrac{1}{2}(3\cos^2\theta - 1), \\ d^{(1)}_{00} &= \cos^2\theta \end{aligned} \tag{2}$$

are the elements of the reduced Wigner matrix for interaction bilinear ($d^{(2)}_{00}$) or linear ($d^{(1)}_{00}$) in the spin operators. This means that by modifying the angle θ from about 54° to 90°, it is possible to switch on or off the secular part of spin interactions, dependent on their rank. Such a possibility has been largely used in the magic angle in the rotating frame (MARF) Imaging [6] as line-narrowing mechanism for large bandwidth sample. The line-narrowing function is set when the matrix elements of Eq. (2) are adjusted to annul the stronger interaction of the sample. Usually that means $d^{(2)}_{00} = 0$, because the dominant interaction in solids is on average dipolar. Because $T_{2\rho}$ depends on the Fourier transform of $\langle F_{lm}(0) F^*_{lm}(t) \rangle$, the correlation function of

* Corresponding author.
E-mail address: francesco.deluca@roma1.infn.it (F. De Luca).

1090-7807/02/$ - see front matter © 2002 Elsevier Science (USA). All rights reserved.
PII: S1090-7807(02)00010-1

the tensor appearing in Eq. (1) keeps up the same properties of orientation-dependence on the transformed Hamiltonian. It has been shown that by $T_{2\rho}$ the ultraslow namics [7] which generally characterizes the molecular mobility of solid-like spin system is detectable.

In this paper, a contrast approach is presented, which supplies the MARF Imaging by a filter based on $T_{2\rho}(\theta, \omega_E)$, namely a filter based on transverse relaxation in the TRF for different values of $\theta(\omega_E)$. The cancellation of the secular dipolar term ($d_{00}^{(2)} = 0$ for $\theta = \theta_{MB} \cong 54°$, the bilinear magic angle value) on solid, as the solid polymers used in this work, allows one to detect the contribution to relaxation from linear terms, as chemical shift anisotropy or spin–rotation and that coming from the nonsecular dipolar terms. While spin–rotation relaxation is particularly active in small, symmetric molecules, in highly entangled polymers the relaxation from chemical shift anisotropy can also be appreciable at low magnetic field when the competitive spin couplings are made weaker. In these systems, the relaxation from chemical shift anisotropy generally derives by the reorientational activity of molecular branches, while that from dipolar interaction is more related to dynamics which involve large segments of the polymer chain [8]. Therefore, the contrast based on this method could allow the individuation of the dominant molecular interactions and dynamics across the sample and correlating them with its macroscopic characteristics. This, in principle, could be also made via the ordinary NMR parameters, but the dominant contribution generally coming from the dipolar interaction flats the T_2 distribution because of the dominant role of the dipolar zero frequency term. On the other hand, T_1 is not enough sensitive to the slow dynamics while $T_{1\rho}$, although sensitive to slow dynamics, is weakly dependent on θ [9,10].

The proposed contrast approach for solid-state imaging could be useful in the characterization of solid polymers or rubbers when it is important to identify changing across the sample after stress testing, or to differentiate areas with amorphous or crystalline structure or areas affected by ageing consequence. All these aspects are, in fact, related to details of the local structure and dynamics to which the $\theta(\omega_E)$-dependent contrast seems particularly sensitive. The spatial characterization of a solid throughout the fine and strong spin interactions distribution can give a view of it that cannot be obtained with other contrast parameters, independently of the NMR Imaging approach. A discussion on the microscopic mechanisms involved in the different Hamiltonians is outside the scope of this work. In this paper, we present a preliminary application of this new contrast approach that shows its experimental practicability and its potentiality on thermally stressed polymers.

2. Experimental results and comments

By modifying the ratio between the radio frequency field intensity and the resonance off-set, the angle θ and therefore the role of the different spin Hamiltonians can be experimentally modified. In particular, for $\theta = \theta_{MB}$, dependent on dynamical condition, the transverse relaxation in the TRF is dominated by chemical shift anisotropy or by the bilinear nonsecular terms. Although higher-order approximation of the $T_{2\rho}$ equation [7], based on the Bloch–Redfield method, shows that at $\theta = \theta_{MB}$ the nonsecular terms of the dipolar Hamiltonian play an important role in giving dependence of $T_{2\rho}$ on slow molecular motion (characteristic correlation time $\tau \approx 10^{-4}$ s) [11,12], in many solids polymers the contribution from chemical shift anisotropy may be detectable in the condition $\omega_E \tau \gg 1$.

In Fig. 1, a couple of rotary echo pulses, which produce the θ-dependent filter, are reported. The filter is composed of two $\vec{B}_E(\theta)$ pulses of the same length τ_E, phase shifted each other by π, and applied after or before the space encoding pulse and, anyway, before the $\pi/2$ read pulse. The $\vec{B}_E(\theta)$ field is produced by a solenoidal coil while the resonance field off-set shift, which it is necessary to get the $\vec{B}_E(\theta)$ inversion, is generated by Helmholtz coils with dc pulse current.

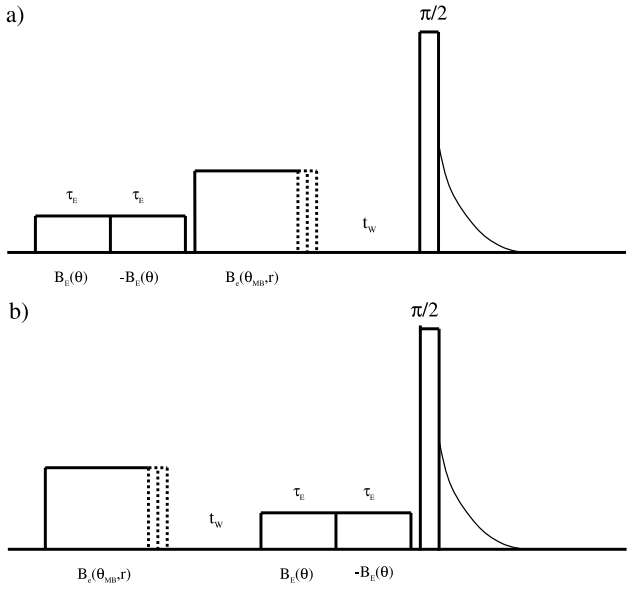

Fig. 1. Pulse sequences used to map solid sample by $T_{2\rho}(\theta, \omega_E)$. The space encoded TRF–FID both in (a) and (b) is reconstructed in the RF by stepping the space-dependent effective field $B_e(\theta_{MB}, r)$. The Fourier transform of the TRF–FID gives the space-dependent $\omega_e(r) = \gamma B_e(\theta_{MB}, r)$ spectrum. In principle, there is no difference between the (a) and (b) sequences until only the maximum echo amplitude is of interest. The condition $T_2 \ll t_W \ll T_1$ must be fulfilled to make the signal amplitude, immediately after the $\pi/2$ pulse, independent of T_2. The sequence used in the present work is that reported in (b).

The rotary echo pulses introduce the operators $\exp[\pm i\omega_E(\theta)\tau_E I_{z'}]$, which describe the $\omega_E(\theta)$ clockwise and anticlockwise rotations of magnetization around the effective field $\vec{B}_E(\theta)$ forming an angle θ with the z-axes. So, the amplitude of the NMR signal from local magnetization is modulated by the term

$$m_+(r,\tau_E) = m_0(r)\exp\left[-\frac{2\tau_E}{T_{2\rho}(B_E(\theta))}\right], \quad (3)$$

where, for the sake of simplicity, a simple exponential form has been assumed for the transverse decay of the TRF signal and where $m_0(r)$ is proportional to the equilibrium magnetization located in $\vec{r}$ [4]. The TRF signal is sampled by measuring the amplitude of the RF signal immediately after the $\pi/2$ pulse, for each step of $B_e(\theta_{MB}, r)$, as shown in Fig. 1. The amplitude of the TRF signal is conditioned by $T_{2\rho}$ which, in turn, depends on the rank of the Hamiltonian selected via θ and by its specific relaxation mechanisms. The effective frequency ω_E associated with the θ-filter can be used as a further parameter by changing $|\vec{B}_E(\theta)|$ and maintaining unvaried its direction in the spin space. The use of ω_E allows exploiting $T_{2\rho}(\theta,\omega_E)$ in its more sensitive range.

The MARF space encoding of the solid sample is realised at $\theta = \theta_{MB}$ by means of an effective field $B_e(\theta_{MB}, r)$ generated by a surface coil (see Fig. 1). In this condition, the interaction of the spin system with the RF gradient produced by the coil (the RF gradient is composed of a dc gradient to form the effective one) assumes the role of dominant interaction [13]. The surface coil has very simple geometry and assures a high radio frequency gradient intensity with good linearity. The best MARF imaging experimental setting allows reaching an effective field intensity of about 2.3 mT with an effective gradient of about 36 mT/m. All the experiments have been performed on samples composed of two pieces of solid polymers arranged as sketched in Fig. 2. The whole volume of the samples is kept as small as possible, compatibly with the SNR criteria, to exploit the best linearity of the effective gradient. The solenoidal and the surface coils have the magnetic axis perpendicular to each other.

In Fig. 3, the profiles obtained on a sample composed of a piece of polyoxmethylene diacetate (PD) and of polyethylene (PE), at different effective field amplitudes, are shown. The RTF echo pulse lengths have been fixed to $\tau_E = 20\,\mu s$. Because of the condition $\theta = \theta_{MB}$, the RTF relaxation is driven by first-rank Hamiltonian and by contribution from the nonsecular dipolar terms. In PD, the relaxation rate $T_{2\rho}^{-1}(\theta_{MB},\omega_E)$ increases suddenly just below about 30 kHz while in PE this happens at about 40 kHz, but with more smooth variation. This effect is well visible on the PD peak, which is dramatically attenuated at $\omega_E = 28$ kHz. The contrast effect is particularly strong if referred to the initial amplitude of the two peaks. The measurements have been made at

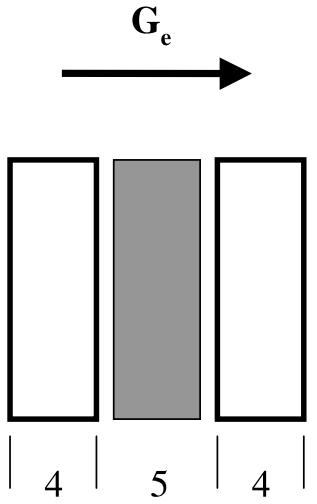

Fig. 2. Sketch of the sample geometry used in the measurements. The dimensions are in millimeter and G_e indicates the direction of the effective field gradient for spatial encoding. The central piece (shaded) is a separator made of teflon.

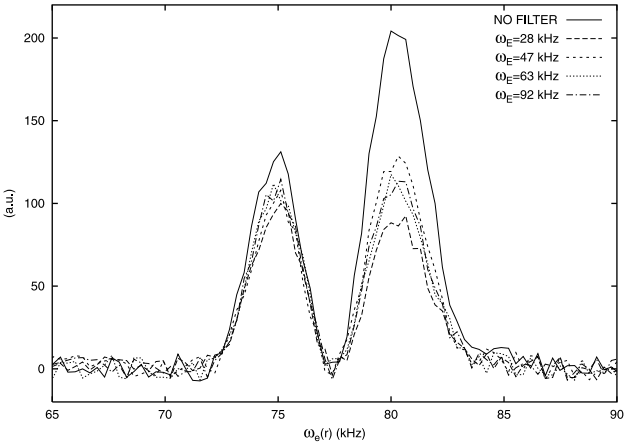

Fig. 3. The spatial profiles of a sample made of polyoxmethylene diacetate (right peak) and of polyethylene (left peak) composed as in Fig. 2 are reported. The profiles are differentiated by ω_E for fixed τ_E and $\theta = \theta_{MB}$. These profiles, as well as all others in the paper, correspond to the rotary echo maximum. The space-encoded frequency $\omega_e(r) = \gamma B_e(\theta_{MB}, r)$ has been obtained with the effective gradient and field given in the text.

room temperature and at a proton Larmor frequency of 30 MHz.

In Fig. 4, the profiles of a sample composed of a piece of PE and of another piece of PE thermally stressed are reported. The stressed PE piece has been heated in a thermal bath at 100 °C for 1 h and then cooled, as fast as possible, to 15 °C. Also in this case, the profiles have been differentiated by ω_E with $\tau_E = 25\,\mu s$ and $\theta = \theta_{MB}$ constant. How it can be seen, the thermal stressed sample has a quite flat dispersion, while the unstressed one follows the same behavior as reported in Fig. 3. The same measurements made on $\theta = \theta_{ML} = 90°$, namely at

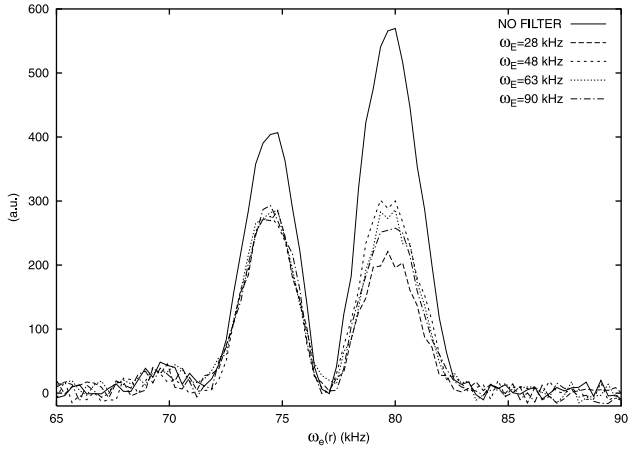

Fig. 4. The spatial profiles of two pieces of polyethylene are reported. The left peak refers to the piece of polyethylene which has been heated for 1 h at 100 °C and then cooled as soon as possible to 15 °C. Also in this case the profiles are differentiated by ω_E for fixed $\tau_E = 25\,\mu s$ and $\theta = \theta_{MB}$. As in Fig. 3, the space-encoded frequency $\omega_e(r)$ has been obtained with the effective gradient and field given in the text.

magic angle for linear interactions, do not show appreciable difference between stressed and unstressed samples. Also, measurements made by the traditional $T_{1\rho}$ are unable to detect difference between stressed and unstressed PE. These results indicate that the thermal stress effect on PE probably involves some structural changes of the solid which are appreciable only in the absence of the strong secular dipolar term. Such alterations probably modify the degree of freedom related to the weaker interactions producing a different behavior of the transverse relaxation.

In Fig. 5, the profiles of two pieces of PD vs θ for different ω_E are reported. The use of the same material to relate profiles obtained with different θ's makes sure that the changes in the orientation of the effective field do not change its spatial distribution. However, only the $T_{2\rho}(\theta, \omega_E)$ data of PD are known with enough details [14] to relate the space-dependent data with the θ-dependent dispersion without space encoding.

In Fig. 5a, the angle between the effective field and the Zeeman field axes is fixed to $\theta = \theta_{MB} \cong 54°$ with $\tau_E = 37\,\mu s$. In this condition, the transverse relaxation rate $T_{2\rho}^{-1}(\theta, \omega_E)$ is rather low, because the contribution comes only from the linear interaction and from the nonsecular terms of the dipolar interaction. The dependence on ω_E shows a sudden change in the relaxation between 19 and 38 kHz, as indicated already in Fig. 3. This change follows the typical spectral density behavior around $\omega_E \approx 1/\tau$. The profiles show no appreciable space-dependent effects because the ω_E dispersion is the same in both peaks. Besides, the ω_E dispersion matches fully with the $T_{2\rho}^{-1}(\theta, \omega_E)$ data obtained without space encoding [14].

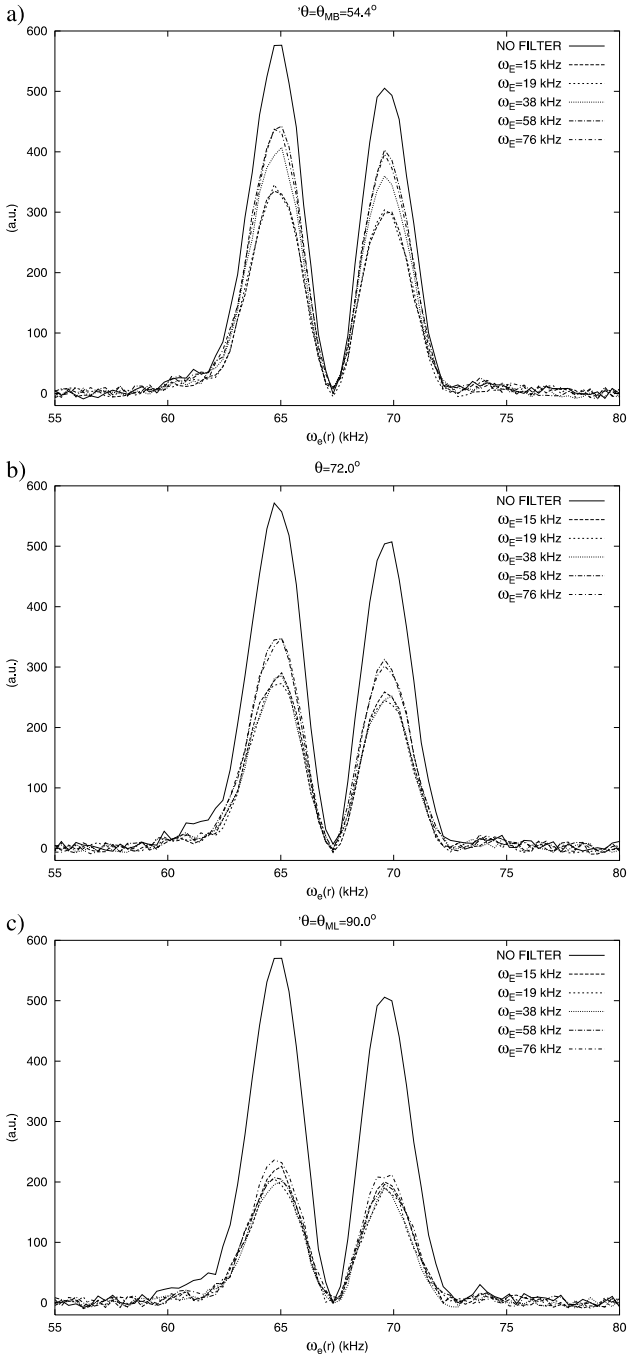

Fig. 5. (a) The profiles of two pieces of polyoxmethylene diacetate obtained with $\theta = \theta_{MB} \cong 54°$ and $\tau_E = 37\,\mu s$ are reported. The dependence on ω_E shows a marked change in the relaxation between 19 and 38 kHz. (b) The angle is fixed to $\theta = 72°$. For this value of θ, the transverse relaxation rate is increased with respect to that of (a) and change between 38 and 58 kHz. (c) $\theta = 90°$; for this value of θ, the transverse relaxation rate is well increased with respect to those reported in (a) and (b) because the relaxation contributions come fully from dipolar interaction being $\theta = \theta_{ML}$, the linear magic angle. The dependence on ω_E shows a small change in the relaxation between 58 and 76 kHz. The space-encoded frequency $\omega_e(r)$ has been obtained with the effective gradient and field reported in the text.

In Fig. 5b, the angle is fixed at $\theta = 72°$ and $\tau_E = 37\,\mu s$. For this value of θ, the transverse relaxation rate is increased with respect to that of Fig. 5a because contributions from the secular term of dipolar Hamiltonian take part in the transverse relaxation. The dependence on ω_E shows a weaker sudden change in the relaxation between 38 and 58 kHz. Also for this value of θ there are no appreciable space-dependent effects and the dispersion matches the data obtained without space encoding.

The highest transverse relaxation rates are those of Fig. 5c. These data have been obtained with $\theta = 90°$ and $\tau_E = 37\,\mu s$. For this value of θ, the transverse relaxation rate is well increased with respect to those reported in Figs. 5a and b because it comes fully from dipolar term, being $\theta = \theta_{ML}$. The dependence on ω_E shows a weaker change in the relaxation between 58 and 76 kHz. Also for this value of θ there are no effects from space encoding.

In Fig. 6, some spatial profiles of Fig. 5 are confronted at the same effective frequency for $\theta = \theta_{ML} = 90°$ and $\theta = \theta_{MB} \cong 54°$. How it can be seen, the variation of the transverse relaxation rate is very different and depends on the effective frequency. Being an extension of the frequency range of $T_{2\rho}^{-1}(\theta, \omega_E)$ different between θ_{ML} and θ_{MB}, the difference in Fig. 6a is lesser than that reported in Fig. 6b for $\omega_E = 58$ kHz. This shows that with this contrast method not only is it possible to make predominant an interaction in the transverse relaxation but also it allows one to select the effective frequency to which the interaction produces its maximum (or minimum) relaxation activity.

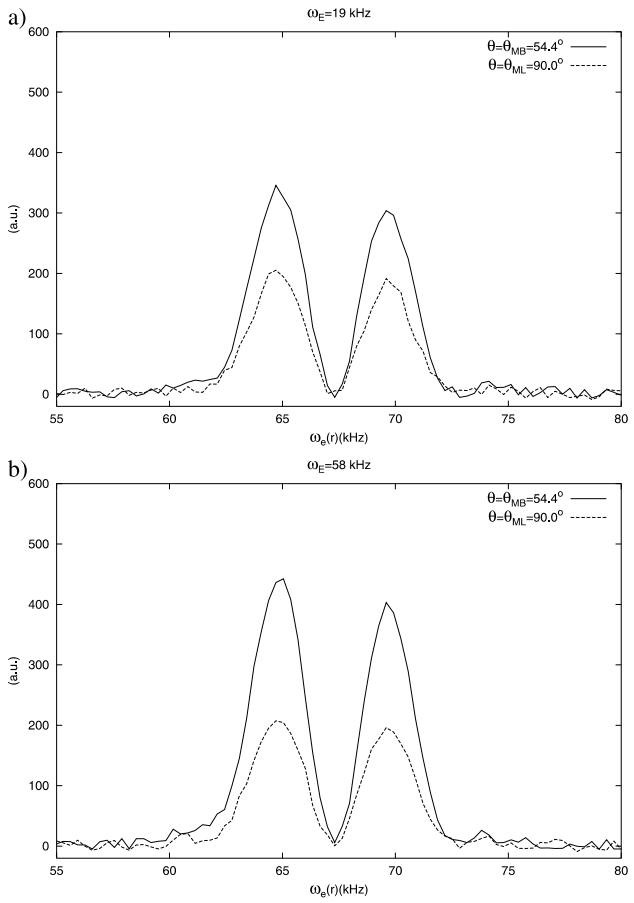

Fig. 6. Some spatial profiles of Fig. 5 are confronted at the same effective frequency for $\theta = \theta_{MB} \cong 54°$ and $\theta = \theta_{ML} = 90°$. (a) The effective frequency is $\omega_E = 19$ kHz, (b) $\omega_E = 58$ kHz.

In this paper, we presented a new approach to contrast solid-state images. It is based on the experimental possibility of choosing the rank of interaction driving the transverse relaxation. The possibility of setting the orientation of the effective field in the TRF, in fact, makes practicable selecting the Wigner matrix element that transforms the spin interaction Hamiltonians from RF to TRF. By the MARF Imaging approach, this contrast can be imaged and therefore the solid-state NMR map can be made sensitive to molecular activity related to certain spin interactions. This aspect, for example, can allow, in favorable condition, to detect degree of freedom related to chemical shift anisotropy, which normally can be observed only in dilute spin system, namely with very weak dipolar coupling. Moreover, the effectiveness of the relaxation can be selected by choosing the effective frequency range in which the relaxation rate is larger (or smaller).

All these possibilities could make the θ-filter utilisable for connecting macroscopic qualities of a sample with its microscopic structures and dynamics. In particular, it can reveal particularly useful information for what concerns the characterization of localized stress processes (mechanical, electrical, etc.) involved in plastics or for the study of space-dependent attributes of glass–rubber transition or about the solidification of polymer melts upon cooling [15], and so on.

References

[1] See for example Solid State NMR, 6 (4) (1996) 275–401 (Special Issue on Magnetic Resonance Imaging of Materials).
[2] B. Blümich, NMR Imaging of Materials, Clarendon Press, Oxford, 2000.
[3] R. Kimmich, NMR Tomography, Diffusometry, Relaxometry, Springer, Berlin, 1997.
[4] F. De Luca, A. Gargaro, B. Maraviglia, G.H. Raza, C. Casieri, Magn. Reson. Imag. 16 (4) (1998) 435.
[5] F. De Luca, E. De Vita, G.H. Raza, C. Casieri, J. Magn. Reson. 139 (1999) 126.
[6] F. Santoro, C. Casieri, F. De Luca, Solid State Commun. 116 (2000) 293.
[7] V.A. Atsarkin, T.N. Khazanovich, Sov. Phys. JETP 60 (1) (1984) 162.
[8] M. Doi, S.F. Edwards, The Theory of Polymer Dynamics, Clarendon Press, Oxford, 1988.
[9] J.S. Blicharski, Acta Phys. Pol. A 41 (1972) 223.

[10] D. Wolf, Spin-Temperature and Nuclear-Spin Relaxation in Matter, Clarendon Press, Oxford, 1979.
[11] V.A. Atsarkin, A.E. Mefed, M.I. Rodak, Sov. Phys. Solid State 21 (1979) 1537.
[12] A.F. Mefed, V.A. Atsarkin, Phys. Status Solidi A 93 (1986) 21.
[13] F. De Luca, G.H. Raza, A. Gargaro, B. Maraviglia, J. Magn. Reson. 126 (1997) 159.
[14] R. Serafini, Thesis, Dipartimento di Fisica, Universita' "La Sapienza" of Rome (2001).
[15] K. Schmit-Rohr, H.W. Spiess, Multidimensional Solid-State NMR and Polymers, Academic Press, San Diego, 1994.